# Growth hormone-releasing hormone attenuates cardiac hypertrophy and improves heart function in pressure overload-induced heart failure

Iacopo Gesmundo[a,1], Michele Miragoli[b,c,d,1], Pierluigi Carullo[b,d], Letizia Trovato[a], Veronica Larcher[b,e], Elisa Di Pasquale[b,d], Mara Brancaccio[f], Marta Mazzola[b,g], Tania Villanova[a], Matteo Sorge[f], Marina Taliano[a], Maria Pia Gallo[h], Giuseppe Alloatti[h], Claudia Penna[i], Joshua M. Hare[j,k,l], Ezio Ghigo[a], Andrew V. Schally[m,n,o,p,2], Gianluigi Condorelli[b,d,q], and Riccarda Granata[a,2]

[a]Division of Endocrinology, Diabetes, and Metabolism, Department of Medical Sciences, University of Turin, 10126 Turin, Italy; [b]Humanitas Research Hospital, 20089 Rozzano (Milan), Italy; [c]Department of Medicine and Surgery, University of Parma, 43126 Parma, Italy; [d]Institute of Genetic and Biomedical Research, National Research Council of Italy, 20089 Rozzano (Milan), Italy; [e]Department of Biotechnologies and Biosciences, University of Milan Bicocca, 20126 Milan, Italy; [f]Department of Molecular Biotechnology and Health Sciences, University of Turin, 10126 Turin, Italy; [g]Division of Cardiovascular Surgery, University of Verona, 37126 Verona, Italy; [h]Department of Life Sciences and Systems Biology, University of Turin, 10124 Turin, Italy; [i]Department of Clinical and Biological Sciences, University of Turin, 10043 Turin, Italy; [j]Interdisciplinary Stem Cell Institute, University of Miami Miller School of Medicine, Miami, FL 33136; [k]Department of Medicine, University of Miami Miller School of Medicine, Miami, FL 33136; [l]Department of Surgery, University of Miami Miller School of Medicine, Miami, FL 33136; [m]Endocrine, Polypeptide, and Cancer Institute, Veterans Affairs Medical Center, Miami, FL 33125; [n]Department of Pathology, University of Miami Miller School of Medicine, Miami, FL 33136; [o]Department of Medicine, Division of Hematology and Oncology, University of Miami Miller School of Medicine, Miami, FL 33136; [p]Department of Medicine, Division of Endocrinology, University of Miami Miller School of Medicine, Miami, FL 33136; and [q]Humanitas University, 20089 Rozzano (Milan), Italy

Contributed by Andrew V. Schally, September 28, 2017 (sent for review July 20, 2017; reviewed by Franco Folli, Steven W. J. Lamberts, and Domenico Salvatore)

**It has been shown that growth hormone-releasing hormone (GHRH) reduces cardiomyocyte (CM) apoptosis, prevents ischemia/reperfusion injury, and improves cardiac function in ischemic rat hearts. However, it is still not known whether GHRH would be beneficial for life-threatening pathological conditions, like cardiac hypertrophy and heart failure (HF). Thus, we tested the myocardial therapeutic potential of GHRH stimulation in vitro and in vivo, using GHRH or its agonistic analog MR-409. We show that in vitro, GHRH(1-44)$NH_2$ attenuates phenylephrine-induced hypertrophy in H9c2 cardiac cells, adult rat ventricular myocytes, and human induced pluripotent stem cell-derived CMs, decreasing expression of hypertrophic genes and regulating hypertrophic pathways. Underlying mechanisms included blockade of Gq signaling and its downstream components phospholipase Cβ, protein kinase Cε, calcineurin, and phospholamban. The receptor-dependent effects of GHRH also involved activation of $G\alpha_s$ and cAMP/PKA, and inhibition of increase in exchange protein directly activated by cAMP1 (Epac1). In vivo, MR-409 mitigated cardiac hypertrophy in mice subjected to transverse aortic constriction and improved cardiac function. Moreover, CMs isolated from transverse aortic constriction mice treated with MR-409 showed improved contractility and reversal of sarcolemmal structure. Overall, these results identify GHRH as an antihypertrophic regulator, underlying its therapeutic potential for HF, and suggest possible beneficial use of its analogs for treatment of pathological cardiac hypertrophy.**

growth hormone-releasing hormone | cardiac hypertrophy | heart failure

Cardiac hypertrophy is initially an adaptive response of the heart to pathophysiologic stimuli, in an attempt to counterbalance ventricular wall stress and preserve cardiac function. However, sustained hypertrophy in response to cardiac insults, such as hypertension or myocardial infarction (MI), can eventually lead to arrhythmias, dilated cardiomyopathy, and heart failure (HF), leading causes of cardiac morbidity and mortality (1). At a cellular level, pathological hypertrophy is characterized by myocyte enlargement and increased protein synthesis, gene-expression reprogramming, and modifications in the sarcomere organization (1, 2). Many pathways are implicated in the transduction of hypertrophic signals, and the initiating stimuli include biomechanical stress and neurohumoral factors, associated with the release of hormones, cytokines, and growth factors by cardiomyocytes (CMs) themselves (2–4). Thus, a major therapeutic strategy in HF is the use of pharmacologic agents aimed at limiting the progression of cardiac hypertrophy. In fact, angiotensin-converting enzyme inhibitors, angiotensin receptor blockers, or β-adrenergic blockers impact on cardiac function by acting on hypertrophy, together with other effects, including those on inotropism (2). These drugs inhibit neuroendocrine signaling, acting also on mechanisms responsible for myocyte growth, cardiac hypertrophy, and HF; however, HF progression is still unavoidable, with a mortality of 50% within 5 y in advanced stages (2, 3). Therefore, identifying new therapeutic

## Significance

Pathological cardiac hypertrophy, characterized by heart growth in response to pressure or volume overload, such as in the setting of hypertension, is the main risk factor for heart failure (HF). The identification of therapeutic strategies to prevent or reverse cardiac hypertrophy is therefore a priority for curing HF. It is known that growth hormone-releasing hormone (GHRH) displays cardioprotective functions; however, its therapeutic potential in hypertrophy and HF is unknown. Here we show that GHRH reduces cardiomyocyte hypertrophy in vitro through inhibition of hypertrophic pathways. In vivo, the GHRH analog MR-409 attenuates cardiac hypertrophy in mice subjected to transverse aortic constriction and improves cardiac function. These findings suggest therapeutic use of GHRH analogs for treatment of pathological cardiac hypertrophy and HF.

Author contributions: J.M.H., E.G., A.V.S., G.C., and R.G. designed research; I.G., M. Miragoli, P.C., L.T., V.L., E.D.P., M.B., M. Mazzola, T.V., M.S., M.T., M.P.G., G.A., and C.P. performed research; M. Miragoli, P.C., M.B., G.A., C.P., J.M.H., A.V.S., G.C., and R.G. analyzed data; and A.V.S., G.C., and R.G. wrote the paper.

Reviewers: F.F., University of Texas Health Science Center and University of Milan; S.W.J.L., Erasmus Medical Center; and D.S., University of Naples Federico II.

Conflict of interest statement: A.V.S. is a coinventor on the Patent for growth hormone-releasing hormone agonists, assigned to the University of Miami, FL, and the Veterans Affairs Medical Center, Miami, FL. J.M.H. owns equity in Biscayne Pharmaceuticals Inc. (Miami, FL). Biscayne Pharmaceuticals did not provide funding for this study.



[1]I.G. and M. Miragoli contributed equally to this work.

[2]To whom correspondence may be addressed email: andrew.schally@va.gov or riccarda.granata@unito.it.

This article contains supporting information online at www.pnas.org/lookup/suppl/doi:10.1073/pnas.1712612114/-/DCSupplemental.

targets to prevent or reverse cardiac hypertrophy may have an impact on survival.

In addition to regulating the release of pituitary growth hormone (GH), GH-releasing hormone (GHRH) exerts many peripheral effects (5, 6), displaying autocrine and paracrine actions and regulating the survival and proliferation of different cell types. Accordingly, the expression of both GHRH and GHRH receptors has been demonstrated in extrapituitary sites (5), including CMs (7–9), skeletal myoblasts, and myotubes (10). We have recently demonstrated the antiapoptotic action of GHRH in H9c2 cardiac cells and adult rat ventricular myocytes (ARVMs), through signaling mediated by the GHRH receptor (GHRH-R) and activation of cAMP/protein kinase A (PKA) (7). GHRH also improved heart function and reduced MI in isolated rat hearts subjected to ischemia/reperfusion (7, 11). Furthermore, synthetic GHRH analogs, with greater activity and metabolic stability compared with native GHRH, were found to promote cardiac repair, improve cardiac function, and reverse ventricular remodeling in rat models of ischemic injury (8, 12, 13), and to reduce MI in swine with ischemic cardiomyopathy (14). Recently, highly potent new GHRH analogs, such as MR-356 and MR-409, have been shown in vitro to reduce calcium influx and promote the survival of H9c2 cardiac cells, and in vivo to reduce rat MI and inflammatory response (9).

These findings suggest that GHRH and its analogs could be useful for therapy of cardiovascular diseases; however, the role of GHRH in cardiac hypertrophy and HF in vivo has not been investigated to date. Hence, in the present study we tested the hypothesis that GHRH would attenuate cardiac hypertrophy. The role of GHRH was assessed in different in vitro models of phenylephrine (PE)-induced hypertrophy, along with the mechanisms involved in these effects. The results obtained from the in vitro experiments were further validated in vivo by investigating the therapeutic action of the GHRH analog MR-409 in a mouse model of pressure overload hypertrophy and HF induced by transverse aortic constriction (TAC).

## Results

**GHRH Attenuates PE-Induced Hypertrophy in Cardiac Cells.** To test the impact of GHRH on hypertrophy, we initially used H9c2 cardiac cells that possess biochemical and electrophysiological characteristics of CMs and similar hypertrophic responses (15, 16). The cells were cultured for 24 h with GHRH at a concentration of 0.5 μM, previously observed to be the most protective against apoptosis (7), alone or with PE (10 and 50 μM). PE, but not GHRH, increased cell surface area, whereas pretreatment with GHRH blocked this effect (Fig. S1*A*). GHRH also lowered the expression of hypertrophic markers *NPPA* and *MYH7*, encoding atrial natriuretic peptide and β-myosin heavy chain (β-MHC), respectively, both up-regulated by PE (Fig. S1 *B* and *C*).

The GHRH-R antagonist JV-1-36, used at 50 nM, in line with our previous studies (7), had no effect alone; however, it blocked the antihypertrophic action of GHRH in PE-treated cells, suggesting receptor-mediated mechanisms (Fig. S1 *D* and *E*).

**GHRH Inhibits Gq Signaling.** Activation of Gq protein by receptors, such as $\alpha_1$-adrenercic receptors ($\alpha_1$-AR), promotes cardiac hypertrophy in vivo and in isolated CMs (4). Hence, we tested the capacity of GHRH to inhibit PE-induced Gq/phospholipase Cβ (PLCβ) signaling. The PLC inhibitor U-73122 blocked the increase in *NPPA* and *MYH7* mRNA in PE-treated H9c2 cells, whereas GHRH maintained its antihypertrophic action, suggesting Gq mediated signaling only for PE (Fig. S2 *A* and *B*). Although both GHRH and PE alone increased PLCβ protein, their coadministration reduced PLCβ to control levels (Fig. S2*C*). Similar results were obtained for phosphorylation of PKCε at Ser729 and for calcineurin, downstream targets of PLCβ (Fig. S2 *D* and *E*). GHRH also counteracted the effect of PE on phosphorylation of phospholamban (PLN) at Thr17, dependent on $Ca^{2+}$/calmodulin-dependent protein kinase II (CaMKII) (Fig. S2*F*).

**GHRH Activates Adenylyl Cyclase/cAMP/PKA.** It is known that GHRH-R activates $G\alpha_s$ and adenylyl cyclase (AC)/cAMP/PKA (5–7); moreover, β-AR signaling, mediated by cAMP/PKA, may antagonize $\alpha_1$-AR and CM hypertrophy (17), whereas $\alpha_1$-AR agonists also stimulate β-AR signaling (18, 19). Here, both GHRH and PE alone increased PKA activity; however, this effect was potentiated in cardiac cells costimulated with PE and GHRH. Moreover, the PKA activator, N6-benzoyladenosine-3′-5′-cAMP (6-Bnz-cAMP), and the AC activator forskolin (FSK) increased, whereas the PKA inhibitor, KT5720, reduced PKA activity (Fig. S3*A*). Accordingly, GHRH also promoted the PKA-dependent phosphorylation of PLN at Ser16, whereas PE had no effect, both alone and in combination with GHRH (Fig. S3*B*). FSK inhibited the increase in *NPPA* and *MYH7* by PE, but potentiated the antihypertrophic effect of GHRH (Fig. S3 *C* and *D*); this, in turn, was inhibited by KT5720, which had no effect on PE alone (Fig. S3 *E* and *F*). Thus, the antihypertrophic action of GHRH involves AC/cAMP/PKA signaling and, although elevated by PE, PKA is not implicated in the hypertrophic effect of PE.

**GHRH Counteracts PE-Induced Increase in Epac1.** Increase in exchange protein directly activated by cAMP1 (Epac1) is involved in cardiac hypertrophy, HF, and arrhythmogenesis through β-ARs signaling (20–23). Here, PE, but not GHRH, increased *Epac1* mRNA in H9c2 cells, an effect abolished by GHRH (Fig. S4*A*). The PKA activator 6-Bnz-cAMP, ineffective on Epac1 (24), blocked PE-induced increase in *Epac1* and potentiated the inhibitory action of GHRH on *Epac1* reduction (Fig. S4*B*). Both the inhibitor of *Epac1*, ESI-09, with no activity on PKA (22), and the $\beta_1$-AR antagonist metoprolol, blocked the PE-induced elevation of *Epac1*, *NPPA*, and *MYH7*, with no effect on the antihypertrophic action of GHRH (Fig. S4 *C*–*H*). These results suggest that GHRH blocks the increase in *Epac1* and counteracts the hypertrophic action of PE through mechanisms mediated by cAMP and PKA.

**GHRH Attenuates Hypertrophy in ARVMs and Human Induced Pluripotent Stem Cell-Derived CMs.** The antihypertrophic effect of GHRH was then tested in ARVMs and human induced pluripotent stem cell-derived CMs (iPSC-CMs). ARVMs, cultured for 24 h with PE, showed increased cell surface area. This effect was attenuated by pretreatment with GHRH (Fig. 1*A*), which also reduced the increase in *NPPA* and *MYH7* mRNA (Fig. 1 *B* and *C*). Moreover, GHRH counteracted the up-regulation in *Epac1* by PE, while having no effect alone (Fig. 1*D*). Human iPSC-CMs showed expression for pituitary *GHRH-R* and *GHRH*, but not for the receptor splice variant *SV1* (Fig. 1*E*). Treatment with PE for 24 h increased mRNA levels of *NPPA*, *NPPB* (encoding brain natriuretic peptide), and *Epac1*; these effects were abolished by cotreatment with GHRH (Fig. 1 *F*–*H*).

**MR-409 Improves Cardiac Function and Remodeling in Pressure Overload-Induced HF.** The effect of the synthetic agonistic analog of human GHRH, MR-409, was tested in the TAC-induced pressure overload model of HF. At 4-wk, TAC mice displayed a significant depression of cardiac function, as evaluated by echocardiographic parameters [i.e., ejection fraction and fractional shortening (FS)]. MR-409 was given 2 wk after TAC, when mice had developed left ventricular hypertrophy and showed a decrease in cardiac function (Fig. 2). Four weeks after TAC, the decrease of FS, the progressive left ventricular dilation, and the transition from concentric to dilated hypertrophy in left ventricles were hindered by the treatment with MR-409 (Fig. 2*B* and Table 1). At 4-wk after TAC, H&E staining showed that the hearts from MR-409–treated mice were smaller compared with those of TAC control (Fig. 3*A*, *Upper*). Cross-sectional area

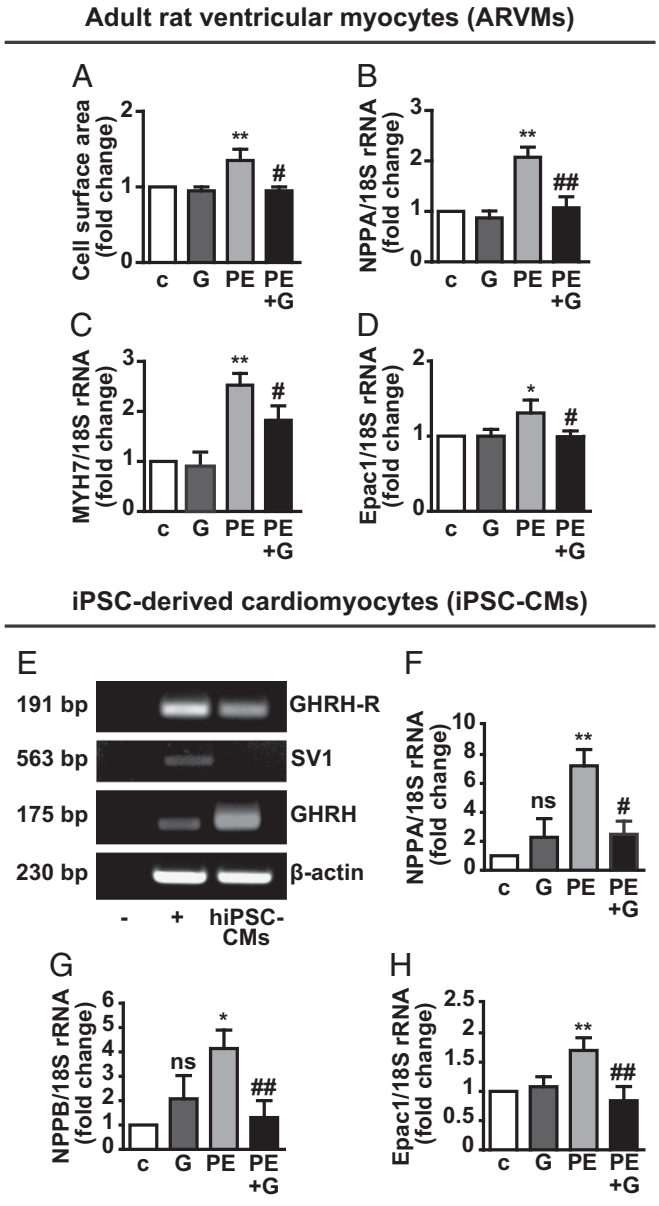


**Fig. 1.** Antihypertrophic effect of GHRH in ARVMs and human iPSC-CMs. Serum-starved ARVMs were treated with GHRH (0.5 μM) and PE (10 μM) for 24 h, alone or with GHRH for 40 min, then with PE for 24 h. (*A*) Cell surface area measured on α-actinin–stained cells. The relative area, normalized to the control, was analyzed in at least 50 cells for each condition in three different fields. (*B–D*) Real-time PCR for *NPPA*, *MYH7*, and *Epac1* normalized to 18S rRNA. For *A–D*, results, expressed as fold-change of control (c), are mean ± SEM $^{*}P < 0.05$ and $^{**}P < 0.01$ vs. c; $^{\#}P < 0.05$ and $^{\#\#}P < 0.01$ vs. PE; $n = 3$. (*E*) Representative RT-PCR showing mRNA for *GHRH-R*, *SV1*, and *GHRH* in human iPSC-CMs. Buffer alone was used as negative control (–). LNCaP human prostate cancer cells were used as positive control (+) and β-actin as internal control. *NPPA* (*F*), *NPPB* (*G*), and *Epac1* (*H*) mRNA assessed by real-time PCR in cells treated for 24 h with 0.5 μM GHRH and 100 μM PE, alone or in combination. Results, normalized to 18S rRNA, are expressed as fold-change of control (c) and are mean ± SEM $^{*}P < 0.05$ and $^{**}P < 0.01$ vs. c; $^{\#}P < 0.05$ and $^{\#\#}P < 0.01$ vs. PE; ns, not significant vs. c; $n = 3$.

analysis in isolated CMs revealed a reversal in myocyte enlargement in TAC mice treated with MR-409 compared with untreated (Fig. 3*A*, *Lower*, and 3*B*), whereas expression of markers of fibrosis and apoptosis was unchanged (Fig. S5 *A–E*). mRNA for *NPPA* and *NPPB* was reduced in CMs of TAC mice treated with MR-409, whereas *MYH6* (encoding α-MHC) and *Acta1* (encoding skeletal α-actin) levels were unchanged (Fig. 3*C*). MR-409 also counteracted the effect of TAC on increase in Epac1, and up-regulated the expression of sarco/endoplasmic reticulum $Ca^{2+}$ ATPase 2a (SERCA2a), that was reduced by TAC (Fig. 3*D*). The serum levels of GH and IGF-I, measured at the end of 4-wk TAC, were unchanged in both sham- and TAC-operated mice treated with MR-409 (Fig. S5 *F* and *G*).

**MR-409 Promotes the Normalization of Contractile Responses in TAC CMs ex Vivo.** A feature of the reverse-remodeled heart is the recovery of contractile responses in isolated CMs, which are blunted during HF (25). Thus, the effect of MR-409 was next studied on the contractility of CMs isolated from TAC mice. Chronic treatment with MR-409 improved both cell shortening at all stimulation frequencies (Fig. S6*A*) and velocity of cell relaxation (Fig. S6*B*). Similarly, the magnitude of calcium transients ameliorated the rising phase (calculated as percentage from baseline-to-peak) increased for all stimulation frequencies, suggesting an improved release of calcium ions from the sarcoplasmic reticulum (Fig. S6*C*). Consequently, the "falling phase"

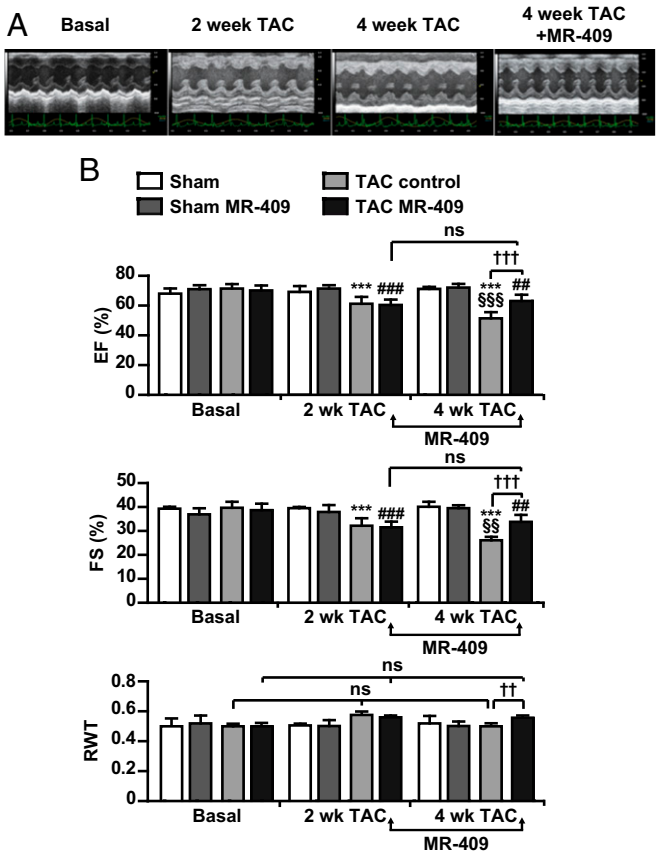


**Fig. 2.** Antihypertrophic effect of MR-409 in vivo. After 14 d, mice subjected to sham operation or TAC underwent echocardiography analysis for heart function and pressure gradient. Only mice with gradients between 60 and 90 mmHg were included in the experiment. Two weeks (wk) after the operation, mice were subcutaneously injected with MR-409 (500 μg/kg/d for 14 d) or vehicle. (*A*) Representative M-mode left ventricular echocardiographic recording at baseline, 2 wk post-TAC, 4 wk post-TAC, and 4 wk post-TAC with MR-409. (*B*) Echocardiographic data: EF%, percent ejection fraction and FS (%), percent fractional shortening, as parameters of left ventricle contractile function; RWT, relative wall thickness. Arrows indicate the time of MR-409 administration (from 2 to 4 wk after TAC). Results are mean ± SEM $^{***}P < 0.001$ vs. TAC Basal; $^{\#\#}P < 0.01$ and $^{\#\#\#}P < 0.001$ vs. TAC MR-409 basal; $^{\S\S}P < 0.01$ and $^{\S\S\S}P < 0.001$ vs. TAC control 2 wk; $^{\dagger\dagger}P < 0.01$ and $^{\dagger\dagger\dagger}P < 0.001$; ns, not significant (Sham, $n = 5$; Sham MR, $n = 5$; TAC, $n = 8$; Tac MR, $n = 9$).

**Table 1. Echocardiographic analysis at basal, 2-wk, and 4-wk Sham and TAC mice treated with MR-409**

| | Basal | | | | 2 wk | | | | 4 wk | | | |
|---|---|---|---|---|---|---|---|---|---|---|---|---|
| Parameter | Sham | Sham MR | TAC control | TAC MR | Sham | Sham MR | TAC control | TAC MR | Sham | Sham MR | TAC control | TAC MR |
| BW, g | 25.6 ± 2.1 | 25.8 ± 1.095 | 25.9 ± 2.2 | 26.4 ± 2.1 | 24.7 ± 2.6 | 26.6 ± 1.14 | 26.1 ± 2.0 | 26.6 ± 1.14 | 25.4 ± 2.9 | 28.2 ± 1.1 | 26.1 ± 1.7 | 27.1 ± 2.0 |
| HR M-mode, bpm | 601.8 ± 17.6 | 588 ± 30.34 | 629.3 ± 158.3 | 593.6 ± 42.3 | 597.2 ± 53.7 | 588.8 ± 30.34 | 577.6 ± 55.8 | 523.0 ± 138.0 | 606.6 ± 46.9 | 627.2 ± 35.2 | 560.0 ± 24.6 | 630.1 ± 21.4$^{\dagger\dagger\dagger}$ |
| LVIDd, mm | 3.3 ± 0.1 | 3.312 ± 0.233 | 3.4 ± 0.1 | 3.3 ± 0.2 | 3.22 ± 0.07 | 3.312 ± 0.23 | 3.67 ± 0.28** | 3.54 ± 0.13 | 3.3 ± 0.2 | 3.296 ± 0.14 | 4.1 ± 0.3*** | 3.7 ± 0.2$^{\dagger\dagger\dagger}$ |
| LVIDs, mm | 2.0 ± 0.1 | 2.092 ± 0.225 | 2.0 ± 0.1 | 2.1 ± 0.2 | 1.95 ± 0.04 | 2.058 ± 0.219 | 2.49 ± 0.27*** | 2.43 ± 0.15 | 2.0 ± 0.2 | 1.992 ± 0.07 | 3.0 ± 0.4*** | 2.4 ± 0.3$^{\dagger\dagger\dagger}$ |
| IVSd, mm | 0.9 ± 0.1 | 0.854 ± 0.053 | 0.9 ± 0.0 | 0.9 ± 0.0 | 0.8 ± 0.0 | 0.824 ± 0.05 | 1.0 ± 0.0** | 1.0 ± 0.1 | 0.8 ± 0.0 | 0.87 ± 0.07 | 1.02 ± 0.07*** | 1.02 ± 0.06 |
| IVSs, mm | 1.3 ± 0.1 | 1.232 ± 0.072 | 1.2 ± 0.1 | 1.3 ± 0.1 | 1.2 ± 0.0 | 1.21 ± 0.053 | 1.3 ± 0.1*** | 1.3 ± 0.1 | 1.26 ± 0.06 | 1.222 ± 0.03 | 1.39 ± 0.06*** | 1.40 ± 0.04 |
| PWTd, mm | 0.8 ± 0.0 | 0.858 ± 0.08 | 0.9 ± 0.1 | 0.9 ± 0.1 | 0.8 ± 0.1 | 0.834 ± 0.053 | 1.0 ± 0.1** | 1.0 ± 0.1 | 0.82 ± 0.10 | 0.862 ± 0.01 | 1.01 ± 0.08** | 1.02 ± 0.09 |
| PWTs, mm | 1.2 ± 0.1 | 1.218 ± 0.036 | 1.2 ± 0.1 | 1.2 ± 0.0 | 1.2 ± 0.0 | 1.276 ± 0.043 | 1.4 ± 0.1*** | 1.4 ± 0.0 | 1.26 ± 0.04 | 1.256 ± 0.06 | 1.38 ± 0.13*** | 1.47 ± 0.07 |

Statistical significance was measured by two-way ANOVA. *$P < 0.05$, **$P < 0.01$, ***$P < 0.001$ vs. Basal TAC control; $^{\dagger\dagger\dagger}P < 0.001$ vs. 4 wk TAC control. bpm, beats per minute; BW, body weight; HR, heart rate; IVSDd, interventricular septal end diastole; IVSDs, interventricular septal end systole; LVIDd, left ventricular internal diameter end diastole; LVIDs, left ventricular internal diameter end systole; MR, MR-409; PWTd, posterior wall thickness in end diastole; PWTs, posterior wall thickness in end systole. (Sham, $n = 5$; Sham MR, $n = 5$; TAC, $n = 8$; TAC MR, $n = 9$.)

required more time-to-reuptake calcium ions and store them in the sarcoplasmic reticulum (calculated as percentage from peak to baseline at the 90% of time) at 1, 2, and 3 Hz (Fig. S6*D*). Overall, CMs exposed to MR-409 denoted a decrease in the time of mechanical relaxation but an increase in the time of calcium reuptake (Fig. S6 *B* and *D*).

In HF, CMs show a typical alteration in morphology and organization of cell membrane transverse tubules (T-tubules) (26) that can be studied by hopping probe scanning ion-conductance microscopy (HPICM), for topographical evaluation of cell membrane organization at nanoscale resolution (27, 28). HPICM revealed a recovery of the alternating *z*-groove and crest morphology on the surface of CMs from TAC mice treated with MR-409, compared with CMs from TAC control mice, which showed less-striated membrane topography. An increase, from 0.43 ± 0.02 to 0.57 ± 0.05, in the *z*-groove index was observed in CMs from TAC MR-409 compared with TAC control mice (Fig. S7).

## Discussion

Our results demonstrate that GHRH attenuates cardiac hypertrophy under pathological conditions. Indeed, GHRH inhibited PE-induced hypertrophy in H9c2 cardiac cells, as well as in ARVMs and human iPSC-CMs, while its analog, MR-409, recapitulates the same rescuing in vivo.

Of note, although our groups have recently demonstrated the cardioprotective role of GHRH, both in vitro and in vivo (7–9, 11–14), the potential protective effect of the hormone in the context of HF has not been previously investigated. We found that in vitro, GHRH reduced the increase in expression of fetal genes by PE, which are classically associated with the development of pathological, but not physiological hypertrophy (29). The antihypertrophic action of GHRH, dependent on activation of GHRH-R, also included blockade of Gq signaling, induced by PE. In fact, GHRH abolished the increase in PLCβ expression and phosphorylation of PKCε by PE, as well as elevation of calcineurin, and inhibited the CaMKII-dependent phosphorylation of PLN at Thr17. Moreover, although GHRH alone increased PLCβ signaling, its antihypertrophic action was not affected by the PLCβ inhibitor, suggesting that Gq signaling is implicated in other effects of the hormone.

In addition to Gq, our results show that the antihypertrophic action of GHRH involved its canonical pathway, namely the GHRH-R–dependent $G\alpha_s$/cAMP/PKA (5, 7, 10). GHRH enhanced PKA activity, an effect also observed with PE, in line with studies showing that high concentrations of PE may activate β-AR signaling in CMs (18, 19). Interestingly, the combination of GHRH and PE further increased PKA activity, suggesting that PKA is implicated in the antihypertrophic activity of GHRH. Accordingly, β-AR–induced elevation of cAMP/PKA was previously shown to reduce the fetal gene response to $\alpha_1$-AR agonists, including PE, in CMs (17). Moreover, our results show that GHRH, but not PE, promoted the PKA-dependent phosphorylation of PLN at Ser16. In line with these findings, activation of cAMP/PKA by FSK blocked the hypertrophic effect of PE, but potentiated the antihypertrophic action of GHRH. Conversely, inhibition of PKA reduced the antihypertrophic effect of GHRH, while being ineffective on PE, indicating a PKA-mediated effect for GHRH, but not for PE.

To further clarify these mechanisms, we focused on Epac, a direct PKA-independent target of cAMP and a mediator of cardiac hypertrophy, HF, and arrhythmogenesis (20–23), whose expression of the main cardiac isoform, Epac1, has been demonstrated in H9c2 cells as well (20). Epac1 induces hypertrophy in vitro and in vivo through mechanisms mediated by the PKA-independent phosphorylation of PLN on Thr17, as well as $Ca^{2+}$ release, activation of PLCε/PKCε/CaMKII signaling (22, 30),

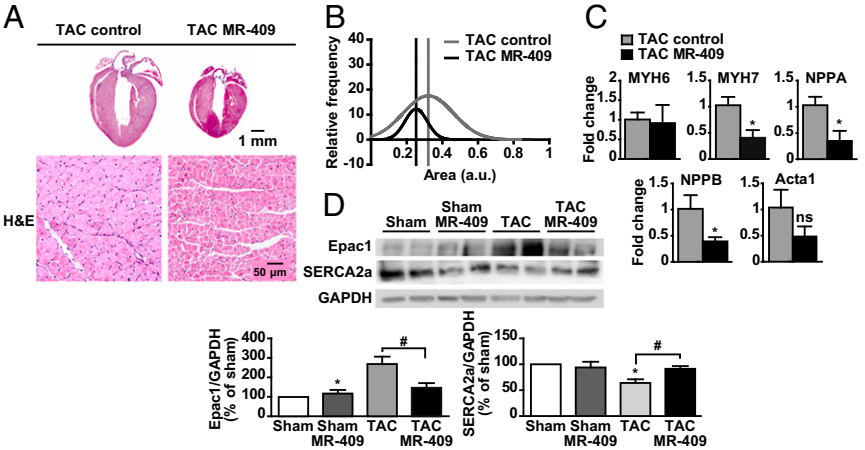


**Fig. 3.** Histological analysis and hypertrophic signaling in TAC mice treated with MR-409. (*A*) Representative mouse heart sections (*Upper*) and CM cross-sectional area (*Lower*) 4 wk after TAC (*Left*, TAC control) or TAC with MR-409 (*Right*) (H&E staining). (*B*) Cell size of single adult CMs from TAC Control and TAC MR-409 mice at 4-wk after TAC ($n = 250$, three mice per group). (*C*) Expression of the indicated genes in CMs from TAC MR-409 and TAC control mice (4-wk). Results, normalized to 18S rRNA, are presented as fold-change vs. TAC control ($n = 3$ mice per group) and are mean ± SEM *$P < 0.05$. (*D*) Representative Western blot for Epac1 and SERCA2a in left ventricles from TAC mice treated with MR-409. Results, normalized to GAPDH and expressed as percent of Sham, are mean ± SEM *$P < 0.05$ vs. Sham; $^{\#}P < 0.05$; $n = 5$.

and elevation of calcineurin and NFAT (21–23). We found that PE increased Epac1 mRNA, an effect abolished by GHRH. Moreover, the PKA activator 6-Bnz-cAMP blocked the increase in Epac1 by PE and potentiated the inhibitory effect of GHRH, consistent with the involvement of PKA in the antihypertrophic action of the hormone. To the best of our knowledge, no studies have previously demonstrated that an $\alpha_1$-AR agonist, such as PE, up-regulates Epac1, which is typically activated by β-AR agonists (23). Accordingly, the increase in Epac1 and the hypertrophic effect of PE, but not the antihypertrophic action of GHRH, were blocked by the Epac1 inhibitor ESI-09, and by the $\beta_1$-AR antagonist metoprolol. Collectively, these findings indicate that, in addition to inhibiting Gq, GHRH blocks hypertrophy in CMs through activation of receptor-mediated cAMP/PKA and inhibition of Epac1, suggesting cross-talk mechanisms between $\alpha_1$- and $\beta_1$-AR pathways (Fig. 4).

The antihypertrophic effect of GHRH was demonstrated also in ARVMs and human iPSC-CMs, along with inhibition in *Epac1* expression, suggesting a potential antihypertrophic action for GHRH in the human heart. In fact, although displaying ultrastructural and electrophysiological properties of immature CMs, human iPSC-CMs are being intensively investigated because of their potential therapeutic applications, specifically in cardiac regeneration and patient-specific cell therapy, representing promising tools for drug discovery and the identification of novel therapeutic molecules (31).

In vivo experiments using the stable agonistic GHRH analog, MR-409, confirmed the potent antihypertrophic properties of GHRH in vitro. Interestingly, as the effect of GHRH(1-44)-$NH_2$ could be reproduced with the analog of GHRH(1-29), MR-409 (13), the active cardioprotective sequence—that is, the part responsible for the cardiac effects—is likely contained in the first 29 amino acids of GHRH.

Importantly, treatment of TAC mice with MR-409 did not just halt disease progression, but rather reversed dysregulated cardiac function. MR-409 even counteracted the effect of TAC on increase in Epac1 and on reduction of SERCA2a expression. Of note, SERCA2a plays an essential role in the contraction and relaxation of cardiac muscle and SERCA2a expression has been shown to be reduced in left hypertrophic ventricles (32). Moreover, in agreement with our previous findings (8, 12, 14), we could not observe elevation of serum GH and IGF-I after administration of MR-409 for 2 wk, suggesting direct cardiac activation. In fact, subcutaneous administration of MR-409 should increase GH levels after 15 and 30 min and last for 30–60 min (13); thus, we cannot exclude an initial raise in GH. However, the beneficial role of GH on cardiac function is controversial (8, 33), whereas the receptor-mediated cardioprotective effects of GHRH and its analogs have been clearly demonstrated, in support of a direct antihypertrophic action of MR-409. Furthermore, it cannot be excluded that in our model of cardiac hypertrophy MR-409 may stimulate the regeneration of cardiac stem cells, since it has been recently demonstrated that GHRH-R agonists, including MR-409, promote the proliferation and survival of cardiac stem cells in vivo and in vitro (8, 12).

The effects on cardiac function in vivo were confirmed by ex vivo experiments in isolated CMs, where MR-409 potently increased inotropic and lusotropic parameters. A similar beneficial effect on signaling and, consequently, on cardiac function has been described for β-AR normalization induced by β-AR blockers in HF (34). From the morphological side, we observed, in the same treated CMs, a plasticity of the cell surface in terms of an increment in *z*-groove ratio compared with untreated TAC cells. These results recapitulated what was recently demonstrated through AAV9.SERCA2a gene therapy for HF by our group: that is, reappearance of *z*-grooves and T-tubules and $\beta_2$-AR relocalization in the reverse remodeled hearts (35).

In summary, our study demonstrates that GHRH and its analog MR-409 not only counteract maladaptive hypertrophy under pathological conditions, but also improve cardiac function in a model of HF with reduced ejection fraction. These findings have important therapeutic implications for disorders characterized by cardiac hypertrophy and HF, since they establish GHRH agonists as novel regulators of hypertrophy and strongly support further translational testing for the treatment of HF.

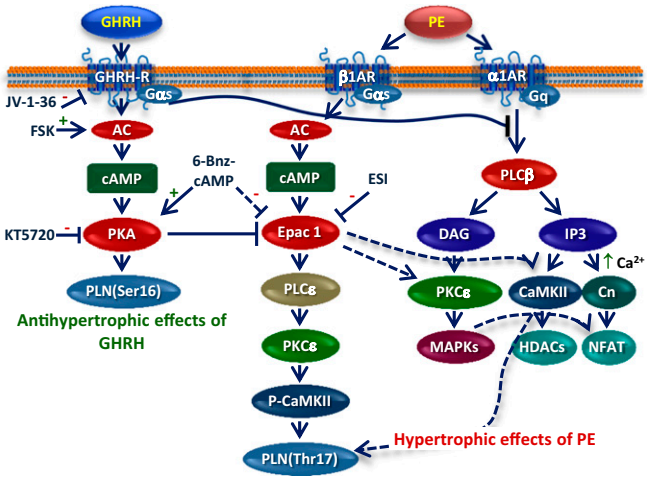


**Fig. 4.** Signaling pathways involved in the antihypertrophic effects of GHRH in vitro. Antihypertrophic actions of GHRH include GHRH-R–dependent activation of the AC/cAMP/PKA pathway (*Left*). GHRH inhibits PE-induced signaling by blocking the $\alpha_1$-AR/Gq pathway and its downstream effectors (*Right*). GHRH also counteracts the increase in Epac1 by PE through activation of PKA and inhibition of Epac1-induced hypertrophic pathways (*Center*). Cross-talk mechanisms between $\beta_1$-AR/$G\alpha_s$/Epac1 and $\alpha_1$-AR/Gq signaling are shown. "+" and "−" indicate stimulatory and inhibitory effects, respectively; interrupted lines indicate indirect effects. Abbreviations: Cn, calcineurin; DAG, diacylglycerol; Epac1, exchange protein directly activated by cAMP; GSK-3β, glycogen synthase kinase-3 β; HDACs, class II histone deacetylases; IP3, inositol trisphosphate; MAPKs, mitogen-activated protein kinases; NFAT, nuclear factor of activated T cells; PLN(Ser16) phospholamban at serine 16; PLN(Thr17) phospholamban at threonine 17.

## Methods

**Cell Lines and Reagents.** H9c2 cardiac cells were cultured as described previously (7). Rat, human, mouse GHRH(1-44)-$NH_2$, and JV-1-36 were from Phoenix Pharmaceuticals. Synthesis and purification of MR-409 [*N*-Me-Tyr$^1$, D-Ala$^2$, Orn$^{12}$, Abu$^{15}$, Orn$^{21}$, Nle$^{27}$, Asp$^{28}$)-hGHRH(1-29)NH-$CH_3$)] in the laboratory of A.V.S. has been described previously (13).

**Isolation of ARVMs.** ARVMs were obtained from young adult rats (1–3 mo) by enzymatic dissociation and cultured as described previously (7). All procedures were approved by the Animal Care and Use Committee of the University of Turin, in accordance with the European Directive 2010/63/EU.

**Generation of iPSC-CMs.** iPSC-CMs were differentiated from human iPSCs previously generated from skin fibroblasts of healthy individuals, as described previously (36).

**Cell Surface Area.** ARVMs were fixed with paraformaldehyde and stained with α-actinin antibody (1:800), then with Alexa Fluor-546 antibody (1:450; Life Technologies). Analysis was performed using an Olympus Fluoview 200 confocal head with an Ar/Kr laser (488 and 568 nm; magnification, 60×) and area calculated using ImageJ software.

**RT-PCR and Real-Time PCR.** RT-PCR and real-time PCR analysis were performed as described previously (7, 10). The primer sequences and amplification products are described in Tables S1 and S2.

**Western Blot Analysis.** Western blotting was performed as described previously (10, 37).

**Animals.** All procedures were performed according to institutional guidelines in compliance with national (D.L. N.26, 04/03/2014) and international law and policies (new directive 2010/63/EU). The protocol was approved by the Italian Ministry of Health. TAC or sham surgery was performed in 8-wk-old C57BL/6J male mice as described previously (38). Fourteen days after the operation, mice were subcutaneously injected with MR-409 (500 μg/kg/day for 14 d) or vehicle, and killed 14 d after treatment.

**In Vivo Cardiac Physiology.** Transthoracic echocardiography was performed at baseline, 14 d after the operations, and at the end of treatments in mice anesthetized with 1% isoflurane, as described previously (39). The pressure gradient was measured by Doppler echocardiography.

**Isolation of Adult Mice CMs and Contractility.** CMs were isolated from adult male mice using standard enzymatic techniques and contractility was measured as described previously (38, 40).

**ACKNOWLEDGMENTS.** We thank the Neuroscience Institute of Turin. This work was supported by a European Research Council Advanced Grant (CardioEpigen, 294609), the Italian Ministry of Health (PE-2013-02356818), PRIN (Italian Ministry of Research and Education) 2015583WMX, and Fondazione CARIPLO Grant 2015-0573 (all to G.C.); PRIN 2010-B5B2NL (to E.G.); Fondazione CRT 2015/273 and University of Turin Ex-60% 2014 and 2015 (to R.G.); and NIH Grants R01 HL107110, R01 HL084275, UM1 HL113460, and R01 HL110737 (to J.M.H.). The work in the laboratory of A.V.S. was supported by the Medical Research Service of the Veterans Affairs Department and University of Miami Miller School of Medicine.

1. Hill JA, Olson EN (2008) Cardiac plasticity. *N Engl J Med* 358:1370–1380.
2. Bisping E, Wakula P, Poteser M, Heinzel FR (2014) Targeting cardiac hypertrophy: Toward a causal heart failure therapy. *J Cardiovasc Pharmacol* 64:293–305.
3. van Berlo JH, Maillet M, Molkentin JD (2013) Signaling effectors underlying pathologic growth and remodeling of the heart. *J Clin Invest* 123:37–45.
4. Heineke J, Molkentin JD (2006) Regulation of cardiac hypertrophy by intracellular signalling pathways. *Nat Rev Mol Cell Biol* 7:589–600.
5. Kiaris H, Chatzistamou I, Papavassiliou AG, Schally AV (2011) Growth hormone-releasing hormone: Not only a neurohormone. *Trends Endocrinol Metab* 22:311–317.
6. Granata R (2016) Peripheral activities of growth hormone-releasing hormone. *J Endocrinol Invest* 39:721–727.
7. Granata R, et al. (2009) Growth hormone-releasing hormone promotes survival of cardiac myocytes in vitro and protects against ischaemia-reperfusion injury in rat heart. *Cardiovasc Res* 83:303–312.
8. Kanashiro-Takeuchi RM, et al. (2010) Cardioprotective effects of growth hormone-releasing hormone agonist after myocardial infarction. *Proc Natl Acad Sci USA* 107: 2604–2609.
9. Kanashiro-Takeuchi RM, et al. (2015) New therapeutic approach to heart failure due to myocardial infarction based on targeting growth hormone-releasing hormone receptor. *Oncotarget* 6:9728–9739.
10. Gallo D, et al. (2015) GH-releasing hormone promotes survival and prevents TNF-α-induced apoptosis and atrophy in C2C12 myotubes. *Endocrinology* 156:3239–3252.
11. Penna C, et al. (2013) GH-releasing hormone induces cardioprotection in isolated male rat heart via activation of RISK and SAFE pathways. *Endocrinology* 154: 1624–1635.
12. Kanashiro-Takeuchi RM, et al. (2012) Activation of growth hormone releasing hormone (GHRH) receptor stimulates cardiac reverse remodeling after myocardial infarction (MI). *Proc Natl Acad Sci USA* 109:559–563.
13. Cai R, et al. (2014) Synthesis of new potent agonistic analogs of growth hormone-releasing hormone (GHRH) and evaluation of their endocrine and cardiac activities. *Peptides* 52:104–112.
14. Bagno LL, et al. (2015) Growth hormone-releasing hormone agonists reduce myocardial infarct scar in swine with subacute ischemic cardiomyopathy. *J Am Heart Assoc* 4:e001464.
15. Hescheler J, et al. (1991) Morphological, biochemical, and electrophysiological characterization of a clonal cell (H9c2) line from rat heart. *Circ Res* 69:1476–1486.
16. Watkins SJ, Borthwick GM, Arthur HM (2011) The H9C2 cell line and primary neonatal cardiomyocyte cells show similar hypertrophic responses in vitro. *In Vitro Cell Dev Biol Anim* 47:125–131.
17. Patrizio M, et al. (2008) cAMP-mediated beta-adrenergic signaling negatively regulates Gq-coupled receptor-mediated fetal gene response in cardiomyocytes. *J Mol Cell Cardiol* 45:761–769.
18. Valks DM, et al. (2002) Phenylephrine promotes phosphorylation of Bad in cardiac myocytes through the extracellular signal-regulated kinases 1/2 and protein kinase A. *J Mol Cell Cardiol* 34:749–763.
19. Markou T, Hadzopoulou-Cladaras M, Lazou A (2004) Phenylephrine induces activation of CREB in adult rat cardiac myocytes through MSK1 and PKA signaling pathways. *J Mol Cell Cardiol* 37:1001–1011.
20. Ulucan C, et al. (2007) Developmental changes in gene expression of Epac and its upregulation in myocardial hypertrophy. *Am J Physiol Heart Circ Physiol* 293: H1662–H1672.
21. Morel E, et al. (2005) cAMP-binding protein Epac induces cardiomyocyte hypertrophy. *Circ Res* 97:1296–1304.
22. Lezoualc'h F, Fazal L, Laudette M, Conte C (2016) Cyclic AMP sensor EPAC proteins and their role in cardiovascular function and disease. *Circ Res* 118:881–897.
23. Métrich M, et al. (2008) Epac mediates beta-adrenergic receptor-induced cardiomyocyte hypertrophy. *Circ Res* 102:959–965.
24. Christensen AE, et al. (2003) cAMP analog mapping of Epac1 and cAMP kinase. Discriminating analogs demonstrate that Epac and cAMP kinase act synergistically to promote PC-12 cell neurite extension. *J Biol Chem* 278:35394–35402.
25. Davies CH, et al. (1995) Reduced contraction and altered frequency response of isolated ventricular myocytes from patients with heart failure. *Circulation* 92:2540–2549.
26. Lyon AR, et al. (2009) Loss of T-tubules and other changes to surface topography in ventricular myocytes from failing human and rat heart. *Proc Natl Acad Sci USA* 106: 6854–6859.
27. Miragoli M, et al. (2016) Microtubule-dependent mitochondria alignment regulates calcium release in response to nanomechanical stimulus in heart myocytes. *Cell Rep* 14:140–151.
28. Miragoli M, et al. (2011) Scanning ion conductance microscopy: A convergent high-resolution technology for multi-parametric analysis of living cardiovascular cells. *J R Soc Interface* 8:913–925.
29. Maillet M, van Berlo JH, Molkentin JD (2013) Molecular basis of physiological heart growth: Fundamental concepts and new players. *Nat Rev Mol Cell Biol* 14:38–48.
30. Oestreich EA, et al. (2009) Epac and phospholipase Cepsilon regulate Ca2+ release in the heart by activation of protein kinase Cepsilon and calcium-calmodulin kinase II. *J Biol Chem* 284:1514–1522.
31. Priori SG, Napolitano C, Di Pasquale E, Condorelli G (2013) Induced pluripotent stem cell-derived cardiomyocytes in studies of inherited arrhythmias. *J Clin Invest* 123: 84–91.
32. Qi M, Shannon TR, Euler DE, Bers DM, Samarel AM (1997) Downregulation of sarcoplasmic reticulum Ca(2+)-ATPase during progression of left ventricular hypertrophy. *Am J Physiol* 272:H2416–H2424.
33. Marleau S, Mulumba M, Lamontagne D, Ong H (2006) Cardiac and peripheral actions of growth hormone and its releasing peptides: Relevance for the treatment of cardiomyopathies. *Cardiovasc Res* 69:26–35.
34. Rockman HA, Koch WJ, Lefkowitz RJ (2002) Seven-transmembrane-spanning receptors and heart function. *Nature* 415:206–212.
35. Lyon AR, et al. (2012) Plasticity of surface structures and β(2)-adrenergic receptor localization in failing ventricular cardiomyocytes during recovery from heart failure. *Circ Heart Fail* 5:357–365.
36. Di Pasquale E, et al. (2013) CaMKII inhibition rectifies arrhythmic phenotype in a patient-specific model of catecholaminergic polymorphic ventricular tachycardia. *Cell Death Dis* 4:e843.
37. Penna C, et al. (2014) Overexpression of the muscle-specific protein, melusin, protects from cardiac ischemia/reperfusion injury. *Basic Res Cardiol* 109:418.
38. Greco CM, et al. (2016) DNA hydroxymethylation controls cardiomyocyte gene expression in development and hypertrophy. *Nat Commun* 7:12418.
39. Rusconi F, et al. (2016) Peptidomimetic targeting of Cavβ2 overcomes dysregulation of the L-type calcium channel density and recovers cardiac function. *Circulation* 134: 534–546.
40. Di Mauro V, et al. (2016) Bioinspired negatively charged calcium phosphate nanocarriers for cardiac delivery of MicroRNAs. *Nanomedicine (Lond)* 11:891–906.
41. Lian X, et al. (2013) Directed cardiomyocyte differentiation from human pluripotent stem cells by modulating Wnt/β-catenin signaling under fully defined conditions. *Nat Protoc* 8:162–175.
42. Nakahama H, Di Pasquale E (2016) Generation of cardiomyocytes from pluripotent stem cells. *Methods Mol Biol* 1353:181–190.

# Supporting Information

## Gesmundo et al. 10.1073/pnas.1712612114

### SI Methods

**Reagents.** M1018 medium, phenylephrine, FSK, SYBR Green dye, anti–α-actinin antibody, ESI-09, metoprolol, and cell culture reagents were from Sigma-Aldrich. KT5720 was from Biomol Research Laboratory Inc. (DBA), U73122 and 6-Bnz-cAMP were from Tocris (Space Import Export). P-PKCε (Ser729), Epac1, and SERCA2a antibodies were from Cell Signaling Technology (Euroclone), GAPDH antibody was from Millipore. Calcineurin A antibody was from Abcam. P-phospholamban (Ser16) and P-phospholamban (Thr17), PLCβ, total antibodies, and actin were from Santa Cruz Biotechnology (DBA). RT-PCR and real-time PCR reagents were from Life Technologies. Primers were from IDT (TemaRicerca).

**Cell Lines.** The embryonic rat heart-derived cell line H9c2 was purchased from American Type Culture Collection and cultured as described previously (7). Cells were maintained in 100-mm dishes at 37 °C with 5% $CO_2$ in DMEM with 10% FBS, 4 mM glutamine, 1% penicillin-streptomycin, and grown to subconfluence before experiments.

**Isolation of ARVMs.** ARVMs were obtained from young adult (1–3 mo) rats by enzymatic dissociation and cultured as described previously (7). All procedures were approved by the Animal Care and Use Committee of the University of Turin, in accordance with the European Directive 2010/63/EU. All solutions used for dissociation contained 10 mM butanedionemonoxime (BDM) to inhibit excitation–contraction coupling. Explanted hearts were cannulated via the aorta and perfused at constant flow rate (5 mL/min) with a peristaltic pump for 5 min with 0 $Ca^{2+}$ Tyrode solution. The latter and the following operations were carried out under a laminar flow hood. The heart was then perfused for 2 min with 0 $Ca^{2+}$ Tyrode collagenase and finally with the same Tyrode-collagenase plus 50 μM $Ca^{2+}$, to facilitate cellular dissociation. The heart was detached from the cannula and the ventricles cut away and minced in small fragments. The fragments were collected in Tyrode-collagenase plus 50 μM $Ca^{2+}$ solution and gently mixed. After 10 min, the medium was replaced with Tyrode 50 μM $Ca^{2+}$ and mixed again with ventricular fragments for 10 min. The supernatant (more than 50% rod-shaped cells) was collected, filtered, and exposed to growing concentrations of $CaCl_2$ (from 50 μM to 700 μM) before the cells were used. For experiments, about 10,000 CMs were plated, respectively, on laminin-treated dishes and incubated in M1018 medium with 10 mM BDM Sigma-Aldrich, 100 U/mL penicillin, 100 μg/mL streptomycin, and insulin, transferrin, selenium (1:1,000; Sigma). CMs were then placed in a 37 °C, 5% $CO_2$ incubator, until adhesion occurred, for at least 2 h.

**Staining for α-Actinin and Assessment of Cell Surface Area.** H9c2 cells and ARVMs were grown into glass coverslips in 24-well plates. After 48 h, cells were serum-starved for 24 h and incubated with the different stimuli. Cells were permeabilized with 0.1% Triton X-100 after fixation in paraformaldehyde, blocked in 1% newborn goat serum for 1 h at room temperature, and stained overnight at 4 °C with α-actinin antibody (1:800). The cells were then incubated for 1 h at room temperature with Alexa Fluor-546 antibody (1:450; Life Technologies). For H9c2 cells, nuclei were stained with Hoechst 33258 (1:1,000) for 10 min at 4 °C. H9c2 cells images were taken using a Leica DM200 fluorescent microscope and a Leica DFC340 FX camera (magnification, 100×) and analysis performed with a Leica Suite image analysis software. For ARVMs, images were captured with an Olympus Fluoview 200 confocal head with an Ar/Kr laser (488 and 568 nm; magnification, 60×). Area calculation was performed using a computerized morphometric system (Image J software, https://imagej.nih.gov/ij/), counting 50 cells from at least 20 randomly chosen fields for each condition.

**RT-PCR and Real-Time PCR.** Extraction of total RNA from H9c2 cells, ARVMs, and human iPSC-CMs, and reverse transcription were performed as described previously (7). Briefly, the cDNA was amplified with the AmpliTaq Gold Polymerase in a GeneAmp PCR System (Perkin-Elmer). For GHRH-R and GHRH, a second PCR (40 cycles) was performed on the primary PCR products. The annealing temperature was 64 °C and 65 °C, for the first and the second PCR, respectively, for GHRH-R; 56 °C for both GHRH PCRs, and 62 °C for SV1. The primers, designed using Primer3, spanned the first amplification product (Table S1). β-Actin mRNA served as internal control; the negative control consisted of no RNA. The LNCaP human prostate cancer cell line (American Type Culture Collection) was used as positive control. The PCR products were separated by gel electrophoresis and visualized by ethidium bromide staining. For real-time PCR, cDNAs were treated with DNA-free DNase (Life Technologies) and reaction performed with the SYBR Select Master Mix (ThermoFischer Scientific) using the ABI-Prism 7300 (Applied Biosystems) or ViiA 7 Real Time (Thermo Fisher Scientific). Disruption of isolated mice CMs was performed for 3 min at 30 Hz, using Tissue Lyser (Qiagen), and total RNA extracted using RNeasy Mini Kit (Qiagen); cDNA was synthesized using SuperScript Vilo cDNA Synthesis Kit (Life Technologies). The primer sequences are reported in Table S2. 18s rRNA was used as endogenous control. Relative quantification was performed using the comparative Ct (2–ΔΔCt) method.

**PKA Activity Assay.** Cells were seeded in 100-mm dishes at a concentration of $5 \times 10^5$ cells. After 48 h, cells were serum-starved for 24 h and incubated with the different stimuli for 15 min. PKA activity was measured from cell lysates using the PKA Kinase Activity Assay kit (Abcam), according to the manufacturer's instructions. Relative kinase activity ($Abs_{450}$) was then calculated using the following formula: Av $Abs_{(sample)}$ − Av $Abs_{(blank)}$, where Av $Abs_{(sample)}$ is the average absorbance of the sample, and Av $Abs_{(blank)}$ is the average absorbance of the blank. The blank consisted of the provided kinase assay dilution buffer (no active kinase).

**Western Blot Analysis.** Western blotting was performed as described previously (10). Proteins (50 or 60 μg) were resolved in 10% or 13% SDS/PAGE and transferred to a nitrocellulose membrane. Membranes were incubated with the specific antibody (calcineurin A, Epac1, P-PKCε, P-phospholamban, PLCβ1, SERCA2a) (dilution 1:1,000). Blots were reprobed with total antibodies or actin for normalization. Immunoreactive proteins were visualized using horseradish peroxidase-conjugated goat anti-mouse or goat anti-rabbit (1:5,000) by enhanced chemiluminescence substrate using ChemiDoc XRS (Bio-Rad), densitometric analysis performed with Quantity One software (Bio-Rad). In mouse experiments, hearts were lysed in Tris-buffered saline with 1% Triton X-100, containing Roche complete protease inhibitor mixture, 10 mM NaF, 1 mM PMSF, and 1 mM $Na_3VO_4$. Protein extracts were prepared as previously described

(37). Protein quantifications were performed with Quantity One software (Bio-Rad).

**Generation of Human iPSC-CMs.** iPSC-CMs were differentiated from human iPSCs, previously generated from skin fibroblasts of healthy individuals, as described previously (36). Cardiac induction was performed using a chemically defined and xeno-free protocol adapted from a method by Lian et al. (41) and that relies on modulation of the Wnt pathway (42). Induction of hypertrophy was carried out using 100 μM PE on CM cultures at day 20 after the start of spontaneous contraction. GHRH was administered at the same time at the final concentration of 0.5 μM, alone or with PE.

**Animals.** All procedures on mice were performed according to institutional guidelines in compliance with national (D.L. N.26, 04/03/2014) and international law and policies (new directive 2010/63/EU). The protocol was approved by the Italian Ministry of Health. TAC or sham surgery was performed in 8-wk-old C57BL/6J male mice as described previously (38). Mice were anesthetized by intraperitoneal injection with ketamine (100 mg/kg) and xylazine (10 mg/kg). The pressure load was verified through measurement of the pressure gradient across the aortic constriction with echocardiography (Vevo 2100; VisualSonics). Fourteen-days postoperation, mice underwent echocardiography analysis to evaluate heart function and pressure gradient. Only mice with a gradient between 60 and 90 mmHg were included in the experiment. Fourteen days after operation, mice were subcutaneously injected with MR-409 (500 μg/kg/d for 14 d) or vehicle, and killed 14 d after treatment. The hearts were excised and CMs isolated by enzymatic perfusion of the left ventricle with Liberaze TM (Roche), using a Langerdorff apparatus, as previously described (38).

**Isolation of Adult Mice CMs.** CMs were isolated from adult male mice using standard enzymatic techniques as previously described (38). Freshly isolated CMs were plated at a density of $0.5–1 \times 10^4/cm^2$ in 22-mm coverslips precoated with 20 μg/mL laminin (Life Technologies) in HBSS supplemented with 0.01 mM $CaCl_2$. Coverslips were mounted on a temperature-controlled perfusion chamber (University of Berne, Switzerland) and slowly superfused with HBSS (Sigma) supplemented with 10 mM Hepes, pH 7.4, to reach the final $Ca^{2+}$ concentration of 1.1 mM.

**Cell Contractility.** CMs were freshly isolated from TAC mice (control) and from TAC mice treated with MR-409. Cells were loaded with 1 μM Fura-2 acetoxymethyl (Thermo Fisher Scientific), field stimulated at 0.5, 1.0, 2, and 3 Hz and recorded using an IonOptix System, as previously described (40). The cells were stimulated with depolarized square pulses at 0.5, 1, 2, and 3 Hz and the following parameters were analyzed during contraction/relaxation periods: cell shortening, time-to-baseline calculated at 90%, and baseline percentage to peak for the intracellular calcium transient.

**GH and IGF-I Analysis.** Total blood from the facial vein of TAC mice was collected at the time of killing. Serum, obtained by centrifugation of total blood at $450 \times g$ at 4 °C for 15 min, was stored at −80 °C until analysis. GH and IGF-I were measured using mouse GH ELISA kit (Cusabio, Space Import Export) and mouse IGF-I ELISA Kit (Abcam) respectively, following the manufacturers' instructions.

**Histochemistry and Cell Size Analysis in CMs Isolated from TAC Hearts.** Mouse hearts were harvested and fixed overnight in formalin, followed by paraffin embedding and sectioning. Histochemical analysis was performed on 3-μm-thick paraffin sections and analyzed by staining with H&E using an Olympus VS120 Virtual Slide Microscope. Isolated adult CMs were acquired with a microscope and converted to greyscale. Cells size measurements were performed using Image J software, according to the user's guide.

***Z*-Groove Ratio Analysis.** The *z*-groove ratio was calculated from topographical images ($10 \times 10$ μm) of cells obtained by HPICM with continuous feedback, as previously described (27). The scanned topographical images were used to quantify disruption of surface structural regularity in TAC mice subjected to vehicle (DMSO) or daily injection of MR-409 for 14 d. Briefly, a piezo-controller (ICnano Scanner Controller; Ionscope Ltd) controlled the three-axis (*xyz*) piezo translation stage (Physik 140 Instruments) custom-assembled with 100-μm closed-loop travel range in *x* and *y*, and 50-μm in the *z* direction. The piezo-stage was driven by a high-voltage amplifier (Physik Instruments) connected to a scanner controller (IC-Nano). The pipette electrode head-stage was connected to a Multiclamp 700B (Molecular Devices). The scan head was assembled onto an electrical micromanipulator (Scientifica) based on a motorized platform (Scientifica). Preparations were imaged with a Nikon TE-i inverted microscope (Nikon Corporation). Nanopipettes (~80 MΩ tip-resistance) were pulled from borosilicate glass with O.D. 1.0 mm and I.D. 0.58 mm (Intracell) using a laser puller P-2000 (Sutter Inc.). Nanopipettes were filled with HBSS without calcium (Sigma Aldrich) containing 10 mM Hepes (Lonza), 0.1 mM $Ca^{2+}$, pH 7.4. Low extracellular calcium concentration is imperative for avoiding undesirable contraction during scan acquisition. Surface topographical images were acquired by HPICM at 25 °C in the same HBSS low-calcium solution. Acquisitions were obtained with customized software, and analysis performed with Prism GraphPad software 6.0.

**Statistical Analysis.** Results are presented as mean ± SEM. Significance was calculated by two-tailed Student's *t* test or two-way ANOVA followed by Bonferroni's multiple comparison test for post hoc analysis. Analysis was performed using GraphPad Prism 6.0. Significance was established for $P < 0.05$.

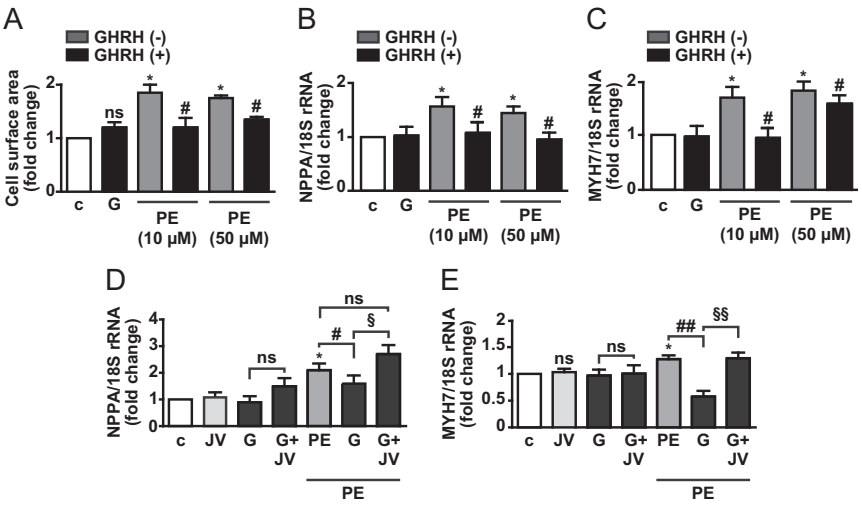


**Fig. S1.** Antihypertrophic effects of GHRH in H9c2 cardiac cells. The cells were serum-starved for 24 h, then incubated with GHRH (0.5 μM) or PE (10 and 50 μM) for 24 h, or preincubated with GHRH for 40 min, then treated with PE for further 24 h. (*A*) Cell surface area measured in cells stained with α-actinin. The relative area, normalized to the control, was analyzed in 50 cells for each condition from at least 20 randomly chosen fields. Results, expressed as fold-change over control, are mean ± SEM $^{*}P < 0.05$ vs. c; $^{\#}P < 0.05$ vs. PE; ns, not significant; $n = 3$. (*B* and *C*) Real-time PCR analysis of *NPPA* and *MYH7* mRNA normalized to 18S rRNA and expressed as fold-change vs. control (c). Results are shown as mean ± SEM $^{*}P < 0.05$ vs. c; $^{\#}P < 0.05$ vs. PE alone, at each concentration; ns, not significant; $n = 3$. (*D* and *E*) *NPPA* and *MYH7* mRNA analyzed by real-time PCR in cells untreated (control, c) or treated for 20 min with JV-1-36 (50 nM), then for 40 min with GHRH (G, 0.5 μM) and for 24 h with PE (10 μM). $^{*}P < 0.05$ vs. c; $^{\#}P < 0.05$; $^{\#\#}P < 0.01$; $^{\S\S}P < 0.01$.

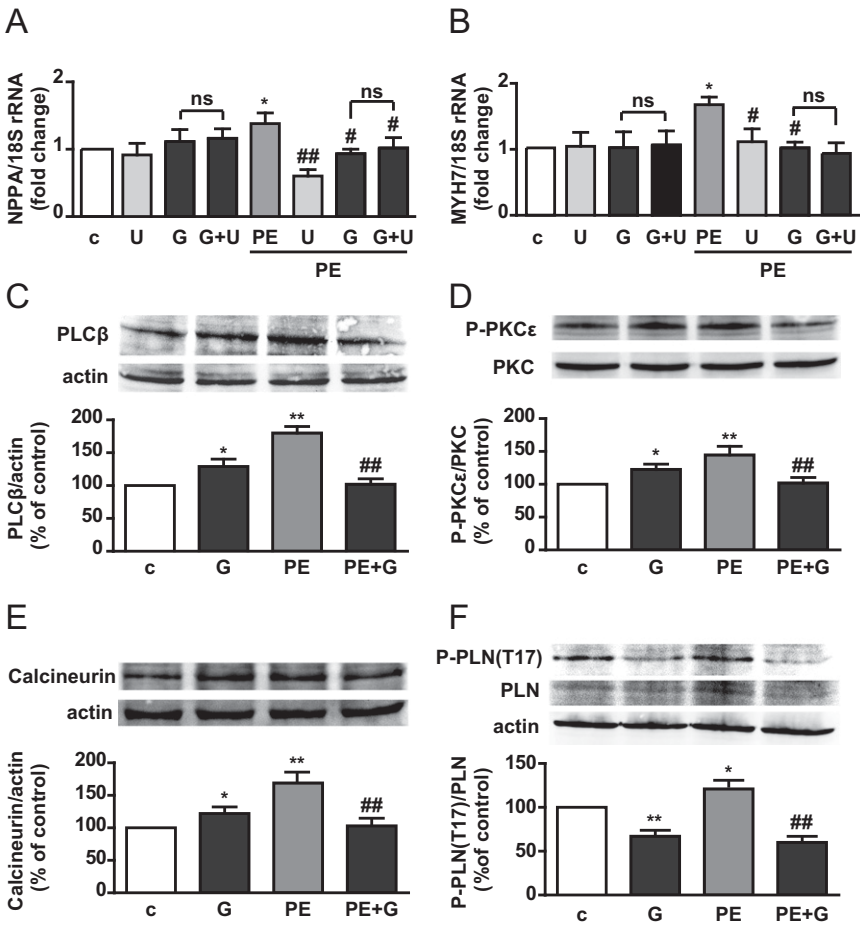


**Fig. S2.** Inhibitory effect of GHRH on PE-induced activation of Gq/PLCβ signaling. (*A* and *B*) *NPPA* and *MYH7* mRNA assessed by real-time PCR in H9c2 cells treated for 20 min with or without 0.5 μM U-73122 (U), then for 40 min with 0.5 μM GHRH and for further 24 h with 10 μM PE. Results, normalized to 18S rRNA, are expressed as mean ± SEM $*P < 0.05$ vs. c; $^{\#}P < 0.05$ and $^{\#\#}P < 0.01$ vs. PE; ns, not significant; $n = 3$. (*C*–*E*) Representative Western blot for PLCβ expression (*C*), PKCε phosphorylation (*D*), and calcineurin expression (*E*) in cells treated for 24 h with the indicated stimuli (*Upper*). Proteins were reprobed with antibody to actin (*C* and *E*) or to total PKCε (*D*) (*Lower*). Graphs show the densitometric analysis of normal or phosphorylated proteins, normalized to actin or their respective total proteins, and reported as percent of basal. Results are presented as mean ± SEM $*P < 0.05$ and $**P < 0.01$ vs. c; $^{\#\#}P < 0.01$ vs. PE; $n = 3$. (*F*) PLN phosphorylation at Thr17 assessed by Western blot in cells stimulated for 30 min with 0.5 μM GHRH, 10 μM PE, or a combination of both (*Top*). Blots were reprobed with antibody to total PLN (*Middle*) and to actin (*Bottom*). Phosphorylated PLN was normalized to total PLN and reported as percent of control. Results are mean ± SEM $*P < 0.05$ and $**P < 0.01$ vs. c; $^{\#\#}P < 0.01$ vs. PE; $n = 3$.

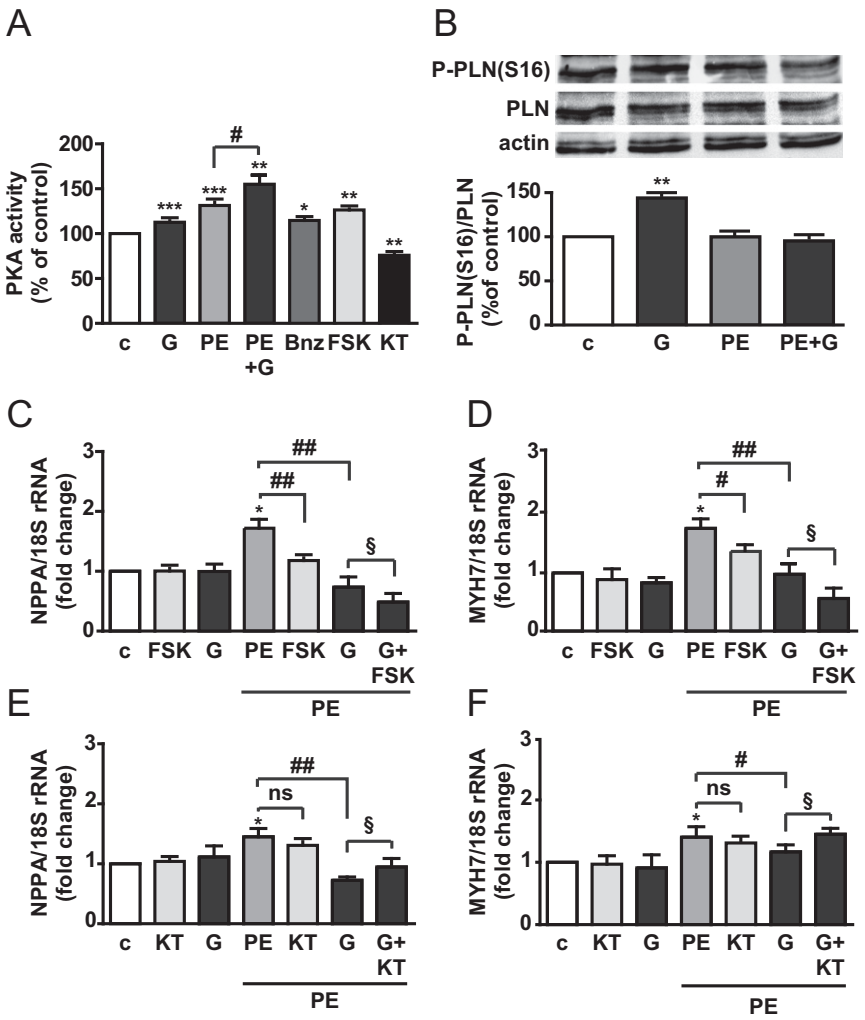


**Fig. S3.** AC/cAMP/PKA-dependent antihypertrophic effects of GHRH. (*A*) PKA activity in H9c2 cells, untreated (control, c) or treated for 15 min with GHRH (G, 0.5 μM) or PE (10 μM), alone or in combination, and with 6-Bnz-cAMP (Bnz, 300 μM), KT5720 (KT, 0.1 μM), or FSK (10 μM). Results are mean ± SEM $^{*}P < 0.05$, $^{**}P < 0.01$ and $^{***}P < 0.001$ vs. c; $^{\#}P < 0.05$; $n = 3$. (*B*) Western blot analysis for PLN phosphorylation at Ser16 in H9c2 cells stimulated for 30 min with 0.5 μM GHRH, 10 μM PE or a combination of both (*Top*). Blots were reprobed with antibody to total PLN (*Middle*) and to actin (*Bottom*). Phosphorylated PLN was normalized to total PLN and reported as percent of control. Results are shown as mean ± SEM $^{**}P < 0.01$ vs. c; $n = 3$. (*C–F*) *NPPA* and *MYH7* mRNA assessed by real-time PCR in cells untreated (control, c) or treated for 20 min with FSK (10 μM) (*C* and *D*) or KT5720 (0.1 μM) (*E* and *F*), then for 40 min with GHRH (G, 0.5 μM), and an additional 24 h with PE (10 μM). Results, normalized to 18S rRNA, are expressed as fold-change over control and are mean ± SEM $^{*}P < 0.05$ vs. c; $^{\#}P < 0.05$, $^{\#\#}P < 0.01$; $^{\S}P < 0.05$; ns, not significant; $n = 3$.

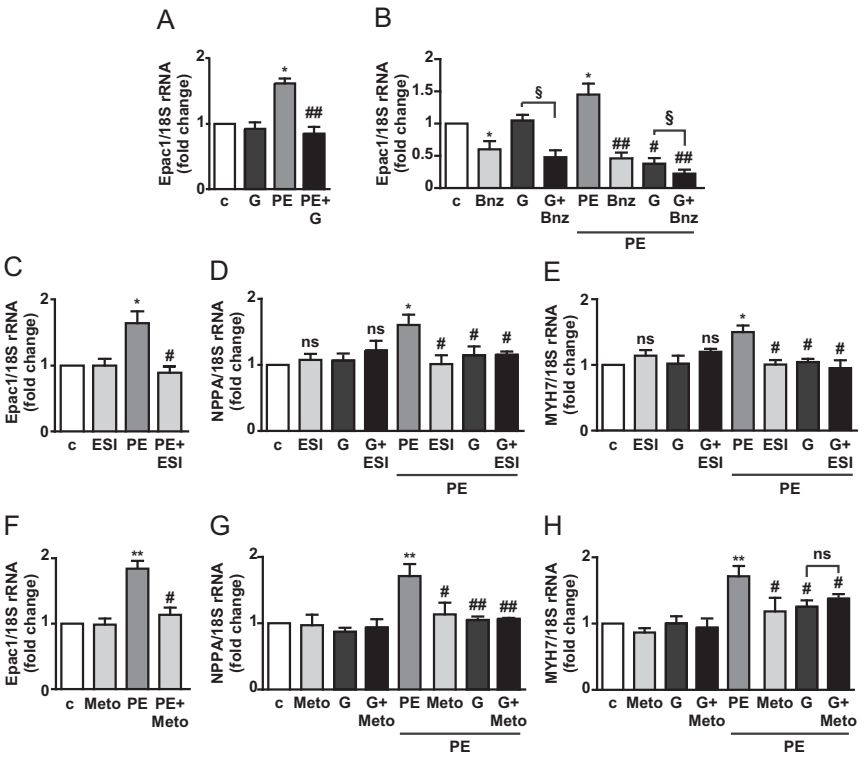


**Fig. S4.** GHRH inhibits PE-induced increase in Epac1. (*A*) *Epac1* mRNA assessed by real-time PCR and normalized to 18S rRNA in H9c2 cells untreated (control, c) or treated for 40 min with GHRH (G, 0.5 μM) and for an additional 24 h with PE (10 μM). Results, expressed as fold-change of control, are presented as mean ± SEM $*P < 0.05$ vs. c; $^{\#\#}P < 0.01$ vs. PE; $n = 3$. (*B*) *Epac1* mRNA assessed by real-time PCR (normalized to 18S rRNA) in cells pretreated for 30 min with 300 μM 6-Bnz-cAMP (Bnz), then for 40 min with 0.5 μM GHRH and for 24 h with 10 μM PE. Results are mean ± SEM $*P < 0.05$ vs. c; $^{\#}P < 0.05$ and $^{\#\#}P < 0.01$ vs. PE; $^{\S}P < 0.05$; $n = 3$. (*C–H*) Real-time PCR for *Epac1*, *NPPA*, and *MYH7* in cells untreated or pretreated for 30 min with ESI-09 (10 μM) (*C–E*), or metoprolol (Meto, 0.1 μM) (*F–H*), then for 40 min with GHRH (G, 0.5 μM) and for an additional 24 h with PE (10 μM). Results, normalized to 18S rRNA, are expressed as fold-change over control and are mean ± SEM $*P < 0.05$ and $**P < 0.01$ vs. c; $^{\#}P < 0.05$ and $^{\#\#}P < 0.01$ vs. PE; $n = 3$.

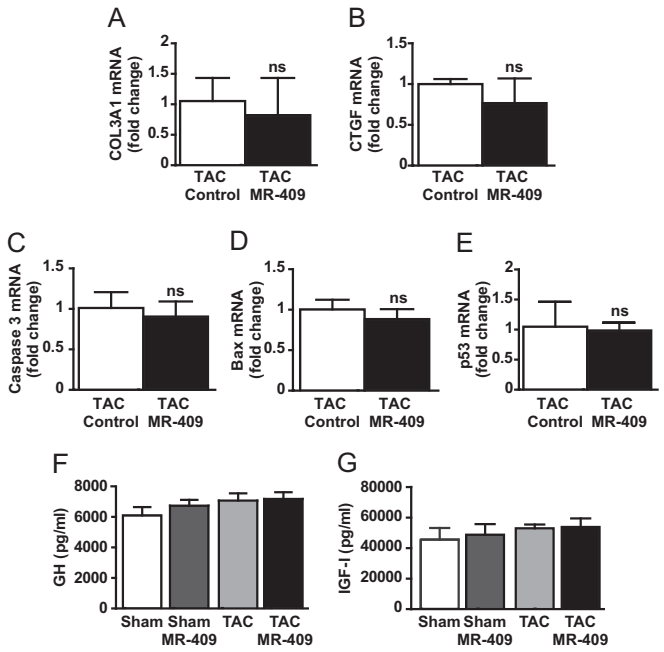


**Fig. S5.** Expression of genes for fibrosis and apoptosis in CMs and serum levels of GH and IGF-I in TAC mice treated with MR-409. CMs were isolated from mice subjected to TAC for 4 wk (TAC control) and from TAC mice treated for 2 wk with MR-409 (TAC MR-409). mRNA levels for collagen type III α 1 chain (COL3A1) (*A*), connective tissue growth factor (CTGF) (*B*), caspase 3 (*C*), Bax (*D*), and p53 (*E*) assessed by real-time PCR and expressed as fold-change of TAC control. Results are mean ± SEM from three independent experiments (ns, not significant). (*F* and *G*) Serum levels of GH and IGF-I determined by ELISA from the facial vein of mice subjected to Sham or TAC for 4 wk, and either untreated or treated for 2 wk with MR-409. Results are mean ± SEM. All results are not significant for Sham MR-409 vs. Sham, for TAC vs. Sham and for TAC MR-409 vs. TAC ($n = 5$, each performed in triplicate).

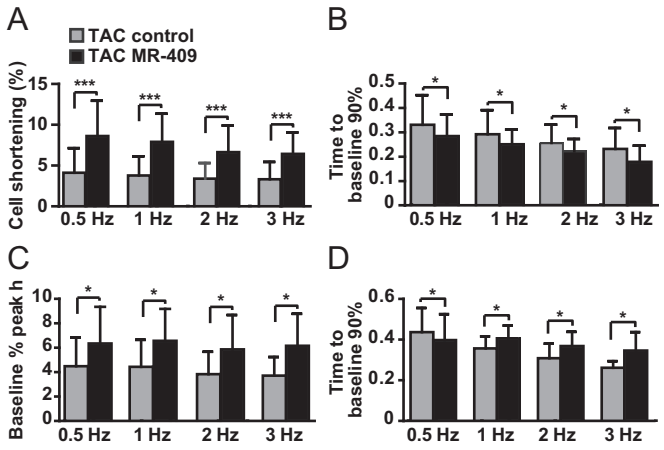


**Fig. S6.** Contractility and calcium transients in CMs from TAC mice treated with MR-409. (*A*) Cell shortening (%) at different stimulation frequencies, $n = 43$. (*B*) Same as *A* for the time-to-baseline calculated at 90%, $n = 43$. (*C*) Baseline percentage to peak for the intracellular calcium transient, $n = 21$. (*D*) Same as *C* for the time-to-baseline (calculated at 90%), $n = 15$. Results are mean ± SEM $^*P < 0.05$; $^{***}P < 0.0001$.

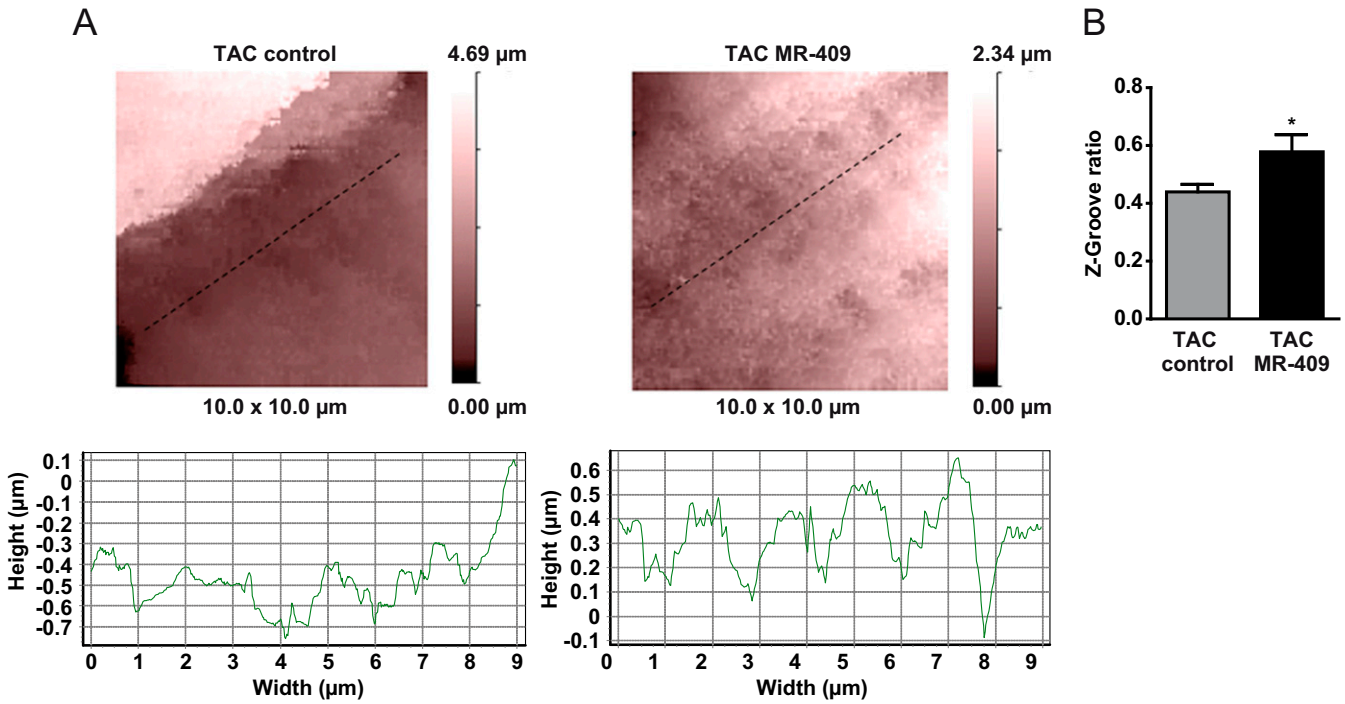


**Fig. S7.** Surface morphology in CMs isolated from TAC mice treated with MR-409. (*A*, *Upper*) Representative SICM image of a ventricular CM isolated from untreated TAC mouse (*Left*, TAC control) and from a TAC mouse treated with MR-409 (*Right*, TAC MR-409). (*Lower*) Surface topographical profiles of crest and *z*-grooved related to a dashed blacked line drawn on the corresponding *Upper* images. (*B*) The *z*-groove ratio calculated from TAC control and TAC MR-409 mice. $n = 13$ for TAC control cells, $n = 11$ for TAC MR-409 cells. Results are mean ± SEM $^*P < 0.05$.

**Table S1. Primers used for RT-PCR analysis**

| Target gene | | | Primer sequence |
|---|---|---|---|
| Human | | | |
| *GHRH-R* (NM_000823.3) | First PCR (322 bp) | Forw | 5′-TTCCTGATCCCACTCTTTGG-3′ |
| | | Rev | 5′-AGCTGCCCAAATTCAAGTGT-3′ |
| | Second PCR (191 bp) | Forw | 5′-CTGCTTCCTCAACCAAGAGG-3′ |
| | | Rev | 5′-AGCTGCCCAAATTCAAGTGT-3′ |
| *GHRH* (NM_021081.5) | First and second PCR (175 bp) | Forw | 5′-AATTGGAGAGCATCCTGGTG-3′ |
| | | Rev | 5′-ACCGGTATGGGGGAATTTTA-3′ |
| *SV1* (XM_011515263) | (523 bp) | Forw | 5′-TGGGGAGAGGGAAGGAGTTGT-3′ |
| | | Rev | 5′-GCGAGAACCAGCCACCAGAA-3′ |
| *β-actin* (NM_001101.3) | (250 bp) | Forw | 5′-GGTCATCTTCTCGCGGTTGGCCTTGGGGT-3′ |
| | | Rev | 5′-CCCCAGGCACCAGGGCGTGAT-3′ |

**Table S2. Primers used for real-time PCR analysis**

| Target gene | | Primer sequence |
|---|---|---|
| Human | | |
| *NPPA* (NM_006172.3) | Forw | 5′-CAGGATGGACAGGATTGGAG-3′ |
| | Rev | 5′-TCCTCCCTGGCTGTTATCTTC-3′ |
| *NPPB* (NM_002521.2) | Forw | 5′-CTTTCCTGGGAGGTCGTTCC-3′ |
| | Rev | 5′-GTTGCGCTGCTCCTGTAAC-3′ |
| *18S* (KU939309.1) | Forw | 5′-CGCAGCTAGGAATAATGGAATAGG-3′ |
| | Rev | 5′-CATGGCCTCAGTTCCGAAA-3′ |
| Rat | | |
| *Nppa* (NM_008725) | Forw | 5′-CTGCTAGACCACCTGGAGGA-3′ |
| | Rev | 5′-AAGCTGTTGCAGCCTAGTCC-3′ |
| *Myh7* (NM_017240) | Forw | 5′-ATCAAGGGAAAGCAGGAAGC-3′ |
| | Rev | 5′-CCTTGTCTACAGGTGCATCA-3′ |
| *Epac1* (XM_008765778) | Forw | 5′-GAGAATGGCTGTGGGAATGT-3′ |
| | Rev | 5′-AGGGGTTCCTCATGGTTAGG-3′ |
| *18S* (X_01117) | Forw | 5′-CCCATTCGAACGTCTGCCCTATC-3′ |
| | Rev | 5′-TGCTGCCTTCCTTGGATGTGGTA-3′ |
| Mouse | | |
| *Myh6* (NM_001164171.1) | Forw | 5′-CGCATCAAGGAGCTCACC-3′ |
| | Rev | 5′-CCTGCAGCCGCATTAAGT-3′ |
| *Myh7* (NM_080728.2) | Forw | 5′-GCATCAAGGAGCTCACC-3′ |
| | Rev | 5′-CTGCAGCCGCAGTAGGTT-3′ |
| *Nppa* (NM_008725.3) | Forw | 5′-GTCAGTCGTTTGGGCTGTAAC-3′ |
| | Rev | 5′-AGACCCAGGCAGAGTCAGAA-3′ |
| *Nppb* (NM_001287348.1) | Forw | 5′-CACAGATCTGATGGATTTCAAGA-3′ |
| | Rev | 5′-CTCATCTTCTACCGGCATC-3′ |
| *Acta1* (NM_001272041.1) | Forw | 5′-CGGGAGAAGATGACTCAAA-3′ |
| | Rev | 5′-GTAGTACGGCCGGAAGCATA-3′ |
| *Caspase3* (NM_001284409.1) | Forw | 5′-AGTCTGACTGGAAAGCCGAAAC-3′ |
| | Rev | 5′-CCACTGTCTGTCTCAATGCCA-3′ |
| *Bax* (NM_007527.3) | Forw | 5′-GGAGATGAACTGGATAGCAATATGG-3′ |
| | Rev | 5′-GTTTGCTAGCAAAGTAGAAGAGGGC-3′ |
| *Col3a1* (NM_009930.2) | Forw | 5′-CCTGGCTCAAATGGCTCAC-3′ |
| | Rev | 5′-CAGGACTGCCGTTATTCCCG-3′ |
| *p53* (NM_001127233.1) | Forw | 5′-GTACCTTATGAGCCACCCGA-3′ |
| | Rev | 5′-CTTCTGTACGGCGGTCTCTC-3′ |
| *18S* (NR_003278.3) | Forw | 5′-GTAACCCGTTGAACCCCATT-3′ |
| | Rev | 5′-CCATCCAATCGGTAGTAGCG-3′ |